Physical Aging and Phase Behavior of Multiresponsive Microgel Colloidal Dispersions

Zhiyong Meng,[†] Jae Kyu Cho,[‡] Victor Breedveld,[‡] and L. Andrew Lyon*[,†]

School of Chemistry and Biochemistry, Parker H. Petit Institute for Bioengineering & Bioscience, and School of Chemical and Biomolecular Engineering, Georgia Institute of Technology, Atlanta, Georgia 30332

Received: November 29, 2008; Revised Manuscript Received: January 22, 2009

Quantitative microscopy measurements have been made on poly(*N*-isopropylacrylamide-*co*-acrylic acid) (pNIPAm−AAc) microgel dispersions as a function of time, temperature, pH, and volume fraction. These studies reveal an extreme degree of complexity in the physical aging and phase behavior of the dispersions; this complexity arises from a convolution of the system energetics at the colloidal, polymer-chain, and molecular scales. Superficially, these dispersions display the classic colloidal phases observed for spherical particles (i.e., gas, fluid, crystal, and glass). However, unlike simple repulsive hard spheres, pNIPAm−AAc dispersions are observed to evolve from a diffusive, fluidlike state immediately after being introduced into rectangular capillary tubes, to very slow crystalline or glassy phases after days or weeks of aging. In addition to this structural evolution, the free volume accessible to the microgels in crystalline or glassy phases (i.e., the cage size) decreases with time, indicating that the physical aging process does not end following assembly, but instead continues to evolve as the dispersion slowly proceeds to an equilibrium state. The temperature dependence of pNIPAm−AAc microgel swelling and how it influences the colloidal assembly was evaluated during the aging process as well. These thermal melting experiments revealed an enhancement in the thermal stability (i.e., a decrease in the influence of temperature on the phase behavior) of the assemblies during the aging process that we associate with an evolution of attractive interparticle interactions during aging. These attractive interactions dictate the time scale for assembly (aging), the final phase adopted by the dispersion, the dynamics of the final state, and the ultimate thermal stability. The culmination of these studies is the pseudoequilibrium phase behavior of pNIPAm−AAc microgel dispersions, which we present as a function of pH and volume fraction following ∼1 month of aging. This diagram reveals highly complex dispersion characteristics that appear to be intrinsically tied to the degree of AAc protonation. In general, we find that, at pH < pK_a, the final dispersions behave in a manner that can be associated with attractive interparticle interactions, whereas at pH > pK_a, repulsive interactions appear to be dominant. These results are discussed in the context of the slow evolution of microgel swelling and attractive interaction potentials arising from reorganization and association of polymer chains via multiple weak hydrogen-bonding interactions.

Introduction

In general, as the volume fraction of colloidal particles is increased, their Brownian dynamics slows from being diffusive to subdiffusive as a result of the formation of transient "cages", which eventually become permanent cages as the particle density increases.[1] When the volume fraction of monodisperse, hard-sphere particles interacting via short-range repulsive potentials reaches the canonical crystallization volume fraction (∼0.494), the particles self-assemble into a crystalline phase in order to maximize their local free volume (i.e., entropically driven assembly).[2] If the volume fraction is increased further, the colloidal system can be forced into a disordered, out-of-equilibrium phase from which it cannot escape on accessible experimental timescales; this kinetically trapped phase is commonly referred to as being jammed or glassy.[3,4] Our groups[5,6] and others[3,7,8] have illustrated, however, that the phase behavior of colloidal dispersions with soft or modulated interactions can be very different from that of repulsive hard spheres as a result of a significant degree of complexity associated with soft interaction potentials,[7,9] as well as the ability to use external triggers such as pH[10−14] and temperature[3,5,8,15,16] to modulate both the interactions and the volume fraction of the spheres.

The intrinsic softness of the interparticle potential between microgels arises from their structure and composition. A microgel is a micrometer- or submicrometer-sized particle composed of a cross-linked polymer network swollen in a good solvent.[16−20] The degree of swelling is governed by the network elasticity,[21] polymer solubility,[22] and solution osmotic pressure.[23,24] Thus, external perturbations that change the solution osmolality or solvent quality will result in a change in microgel swelling (volume). Of the microgels that are extremely sensitive to environmental conditions, the most heavily investigated are those based on poly(*N*-isopropylacrylamide) (pNIPAm) because of the dramatic volume phase transition (VPT) that occurs in such particles near the lower critical solution temperature (LCST) of the polymer.[3,25,26] It has been shown that monodisperse preparations of pNIPAm microgels can self-assemble into colloidal crystalline phases,[3,5,9,10,27−29] which have been applied to sensing,[30,31] photonics,[28,32,33] and the study of fundamental issues in condensed-matter physics.[6,34] The random incorporation of acrylic acid (AAc) moieties, which results in pNIPAm−AAc copolymer microgels, gives rise to particles that are responsive to additional environmental factors, such as pH and ionic

* Corresponding author. E-mail: lyon@gatech.edu.
[†] School of Chemistry and Biochemistry and Parker H. Petit Institute for Bioengineering & Bioscience.
[‡] School of Chemical and Biomolecular Engineering.

10.1021/jp8104979 CCC: $40.75
Published on Web 03/19/2009

strength,[24,35] thus providing additional experimental parameters to control particle assembly. As described in this contribution, the addition of this comonomer also imparts tremendous complexity to the system; as a result, extensive studies were required to even begin to explain the origins, magnitudes, and interplay of the observed phenomena.

The data presented below are the outcome of >8 years of experimentation on the pNIPAm−AAc microgel system. At first glance, this appeared to be a simple and tractable experimental framework within which to study soft colloidal interactions. We initially expected the phase behavior of these colloids to be both pH- and temperature-dependent, with the assembly's responsivity mirroring the response of component particles to the independent stimuli. However, early on, we discovered that the interparticle interactions were far more complex than initially anticipated. In 2003, we first reported the possible existence and origins of attractive particle interactions between pNIPAm−AAc microgels in a series of optical microscopy studies.[5] More precise and detailed studies were reported in 2007, wherein we described the use of quantitative particle tracking studies to elucidate particle dynamics, as well as our initial findings on enhanced thermostability of the colloidal assemblies and its possible connection with attractive interparticle potentials.[6] In this contribution, we attempt to summarize and recast those results in a self-consistent experimental framework; to fully describe the phase behavior of the dispersions as a function of pH and volume fraction; and most importantly, to discuss the time dependence of colloidal assembly and thermostability. The aging of these dispersions is a previously unexplored phenomenon that provides a tremendous amount of insight into the forces that dictate the phase behavior. Importantly, an understanding and appreciation of aging is critical for future studies of these and similar systems, as the measurement of assembly properties becomes a "moving target" that is critically dependent on the initial conditions and history of the sample.

Results and Discussion

As described above, we have previously studied the phase behavior of pNIPAm−AAc microgels as a function of volume fraction and over a limited range of pH values; these studies have revealed some surprising behaviors that are typically interpreted as arising from weak attractive interparticle potentials associated with polymer−polymer hydrogen bonding and, in the case of low particle concentrations, a concomitant microgel swelling that maximizes the number of particle−particle interactions.[5,6] Despite these investigations, we have examined only a small region of phase space and have also largely ignored the time evolution of phases. To fill in these gaps in our knowledge and thereby expand our understanding of this complex colloidal system, we have mapped a wider range of phase space by controlling two parameters: particle concentration and pH. (Experimental details are included in the Supporting Information.) We have also carefully examined the evolution of the different phases as a function of time to observe the pathway taken by the dispersions as they evolve from the initial nonequilibrium state. By doing so, we have made a number of extremely surprising observations related to pNIPAm−AAc microgel dispersions and their aging properties. Perhaps the most obvious evidence for dispersion aging is observable with the naked eye. Figure 1 shows a photograph comparing the appearance of new and aged samples; the left capillary holds a 1-day-old pNIPAm−AAc microgel dispersion (2.0 wt % polymer in pH 3.5 buffer), whereas the right capillary holds an aged (27-day-old) dispersion (2.0 wt % polymer in pH 3.5 buffer). The aged sample clearly shows iridescence under white light illumination due to Bragg diffraction from the colloidal crystalline lattice. Whereas the slow assembly of colloids is not in and of itself surprising, the detailed dynamics and pathway of the assembly are suggestive of an extremely complex colloidal system. Indeed, very surprising results have been obtained from this system that illustrate just how different the physics are from those of repulsive hard-sphere particles.

Figure 1. Aging of pNIPAm−AAc microgel samples at 20.0 ± 0.1 °C as visualized on the macroscopic scale. Both microgel samples contained 2.0 wt % polymer in a pH 3.5 buffer after aging for different periods [left, 1 day (fluid); right, 27 days (crystal)]. The samples were photographed against a white grid to aid in photographic focusing.

The complexity of the system can be understood phenomenologically by considering the additional energy terms that must be considered for microgel dispersions as compared to traditional hard spheres. Whereas hard spheres have a fixed volume that dictates the length scales over which they interact, microgels can swell and collapse to minimize the free energy of the assembly. For example, we and others have shown in the case of purely repulsive microgels that, when the number density of the microgels is increased, the microgels condense to occupy a smaller volume in order to accommodate the additional particles.[9,23] This phenomenon is physically similar to the osmotic deswelling of gels in the presence of a linear polymer[36,37] and to the conformational changes observed for linear polymers as the concentration of polymer is increased (e.g., moving from the dilute to the semidilute regime).[23] From these examples, it is clear that the behavior of microgel dispersions must be interpreted in terms of both their colloidal and polymer solution properties. The solvation, conformation, elasticity, and topology of the polymer chains will contribute to the observed colloidal behavior, as all of these factors dictate how the microgel volume and particle−particle interactions change as a function of microgel concentration, solution conditions, and external stimuli (e.g., temperature). The picture becomes even more complex when weakly attractive interactions are introduced. Now, as the particle concentration (volume fraction) is increased, those interactions must influence not only how the microgels assemble with each other, but also how the microgels swell or collapse in order to minimize the free energy of the system. For example, one could imagine conditions under which the entropic cost associated with swelling the microgels could be compensated by an enthalpic gain from attractive polymer−polymer interactions. Under conditions where the pairwise interactions are weak relative to the thermal energy (kT), such microgel swelling would be particularly important in the stabilization of an assembly, as multibody interactions would be required to overcome Brownian forces. In the results described herein, we illustrate a wide range of behaviors wherein the delicate interplay between the colloidal and polymer energy scales produce complexity that is not observable in the hard-sphere domain. Through careful mapping of this behavior as a function of particle concentration, time, temperature, and pH, a more complete picture of such systems is beginning to emerge.

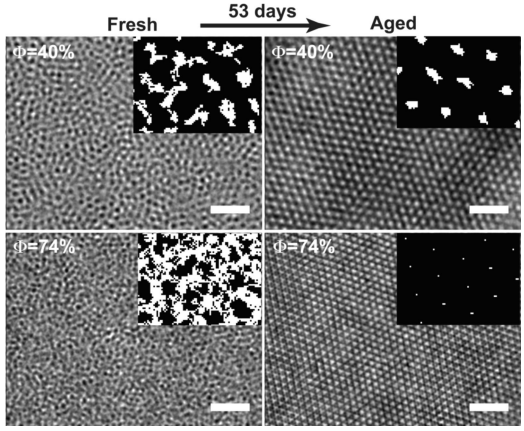

Figure 2. Phase behavior of pNIPAm−AAc microgel dispersions at pH 3.0 and 20 ± 0.1 °C. The volume fractions of the pNIPAm−AAc microgels are displayed at the top left of each image. The top-right inset in each image shows the particle trajectories over ∼10 s of observation. Trajectories are magnified by a factor of 4 relative to the images for ease of trajectory visualization. All scale bars represent 10 μm.

Examples of the complexity in the system are evident in the optical microscopy images and particle trajectories shown in Figure 2. A microgel sample buffered at pH 3.0 with an initial particle volume fraction of 40% is a fluid immediately after preparation. (See the Supporting Information and additional discussion below for details on volume fraction calculations.) This is expected, as the sample lies below the canonical freezing point for spherical colloids. However, after 53 days, the sample has evolved to form a highly ordered crystalline phase wherein the particles appear to be in contact with one another, which should not be possible for a simple repulsive dispersion. This result is an apparent example of the case discussed above, where the ability of the microgels to swell permits the evolution of a close-packed phase from a non-close-packed one. On the other hand, if the initial effective volume fraction of a sample at the same pH is 74% (the packing limit for spherical hard spheres), the sample again is a fluid immediately after preparation. This result is extremely surprising, given the fact that the diffusion of hard spheres is so frustrated at this packing fraction that such concentrations are typically not possible in dispersions because of particle jamming; close-packed hard-sphere assemblies are typically formed by more specialized approaches such as slow solvent evaporation. After 53 days, this sample has completely crystallized to form a close-packed structure, thereby aligning with our preconceived notions of colloidal phase behavior. In this case, the initial state is illustrative of the previously described osmotic deswelling effect,[9,23] wherein the microgels deswell in order to accommodate their neighbors. Despite these phenomenological descriptions, these data illustrate some key questions that need to be addressed experimentally: (1) How can "packed" samples behave as fluids when first prepared, and how can more dilute samples form crystals? (2) What is the pathway by which microgel dispersions age, and what can the pathway tell us about the evolution of the interparticle forces? (3) How do temperature, volume fraction, and pH influence sample aging and the initial and final states?

The data presented in Figure 2 are representative of all samples observed in this work between pH 3 and 4.5 with initial volume fractions between ∼0.35 and 0.74. These samples started as diffusive fluids immediately after preparation and equilibrated to colloidal crystals or crystal/glass mixed phases after aging at room temperature for ∼1 month.[6] At pH 3.5, the aging process is quite slow, and crystallization is favored over a broad range

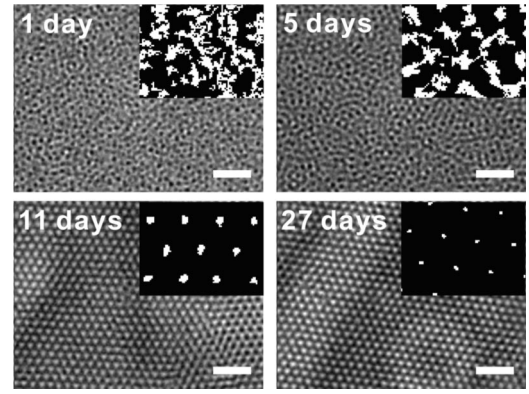

Figure 3. Microscopic images and trajectories (inset, ∼10 s of observation) of pNIPAm−AAc microgel samples (2.0 wt % polymer in pH 3.5 buffer) at different ages (not in the same spot) and 20.0 ± 0.1 °C; aging times are indicated on all microscopic images. Trajectories are magnified by a factor of 4 relative to the images for ease of trajectory visualization. Scale bar = 10 μm.

of volume fractions (vide infra), thereby making these conditions suitable for detailed experimental investigations of the crystallization dynamics; we will therefore focus on experiments at pH 3.5 for the detailed aging studies reported herein. Note, however, that qualitatively similar behavior was found for all microgel samples that we have observed to undergo aging from fluids to glasses or crystals.

More detailed observation of these samples by bright-field video optical microscopy permits a direct determination of the dispersions' structures and the particle dynamics. The bright-field micrographs and trajectories (inset) for a 2.0 wt % polymer in pH 3.5 buffer at different time points are displayed in Figure 3. Note that the inset trajectory maps are magnified by a factor of 4 relative to the bright-field images for easier visualization of the trajectories. The microgel dispersions are fluidlike immediately after sample preparation (1- and 5-day data), with diffuse trajectories and no evidence of spatial order. Eventually, the samples display crystalline order and caged trajectories, which are illustrated here by the 11- and 27-day data. Note that, even after formation of the ordered phase, the particle dynamics continues to evolve, with the particle trajectories becoming more constrained with aging (11- vs 27-day data). In addition to the direct visualization of particle dynamics and spatial organization, the microscopy data can offer a quantitative assessment of the particle diffusion. To illustrate this, a double-logarithmic plot of the particles' mean square displacement (MSD) versus lag time (τ) as a function of the number of days after preparation is shown in Figure 4a (2.0 wt %, pH 3.5). The MSD of microgel particles in an ensemble is given by

$$\mathrm{MSD}(\tau) = \langle [r_i(t + \tau) - r_i(t)]^2 \rangle_{i,t} \quad (1)$$

where $r_i(t)$ is the position vector of the ith particle at time t, τ is the lag time, and $\langle\rangle_{i,t}$ indicates the spatial average over both the ensemble of particles and all starting times t. In the colloidal gas regime, where particle motion is purely diffusive and interactions between particles are negligible, the MSD should be proportional to lag time

$$\mathrm{MSD}(\tau) = 2dD\tau \quad (2)$$

where d is the dimensionality of the displacement vectors and D is the translational self-diffusion coefficient of microgel

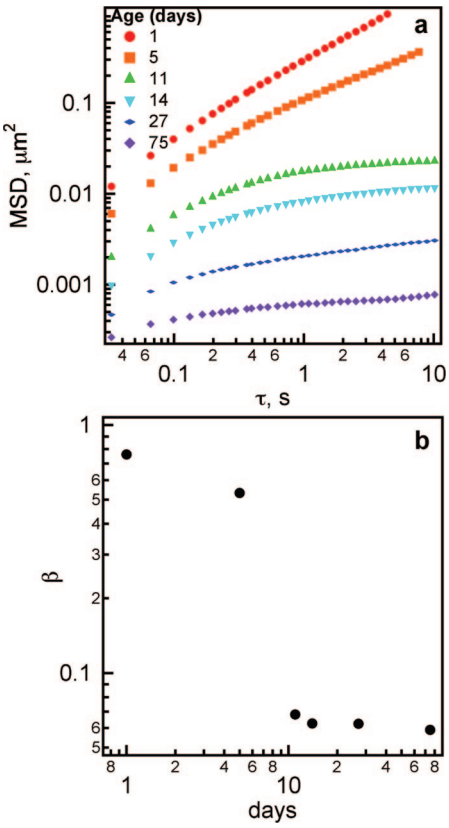

Figure 4. (a) Mean square displacement (MSD) versus lag time (τ) of pNIPAm−AAc microgel particles (2.0 wt % polymer in pH 3.5 buffer) at different ages and 20.0 ± 0.1 °C. (b) Power of the lag time versus age of the pNIPAm−AAc microgel dispersion. MSD ∝ τ^{β}, where β is the power of the lag time.

particles. In general, the MSD of colloidal particles scales with lag time

$$\mathrm{MSD}(\tau) \propto \tau^{\beta} \tag{3}$$

where the scaling parameter β is the slope in a double-logarithmic plot of MSD(τ) versus τ. Generally, $\beta = 1$ for Brownian diffusive motion, whereas β values between 0 and 1 denote subdiffusive behavior. In these studies, β was obtained by regression analysis of MSD(τ) versus τ plots over the range $\tau = 0.1-1$ s. The MSD plots in Figure 4a and the β values in Figure 4b illustrate a marked slowing of particle motion with sample aging: One day after sample preparation, the colloidal dispersion shows nearly diffusive fluid behavior with $\beta = 0.76$. As the sample ages, the maximum MSD of the samples at long lag time decreases, as does the magnitude of β. These data also illustrate that the initial aging is fairly rapid, with the 1-day-old sample showing an MSD of >1 μm^2 at a lag time of 10 s (determined via extrapolation), whereas the 5-day-old sample shows an MSD of ~0.14 μm^2 at 10 s. Thus, during the first 5 days of aging, the maximum particle displacement decreases by about 90%, with the sample progressing from a fast, diffusive fluid to a slow, subdiffusive fluid. When these microgel dispersions were aged for over 7 days, crystallization occurred, with the crystallites initially coexisting with a fluid phase (data not shown). After 11 days of aging, a macroscopic crystalline phase had fully formed, which was observed through the appearance of sample iridescence, as shown in Figure 1. At this point, MSD analysis showed the appearance of a plateau, indicating the formation of permanent cages around the particles,

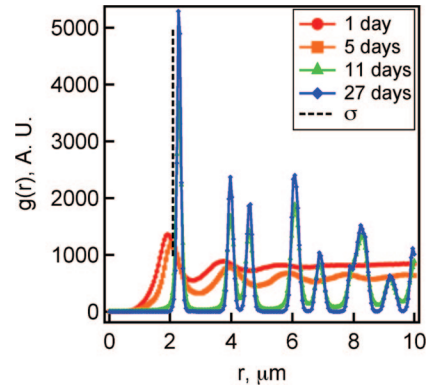

Figure 5. Radial distribution function, $g(r)$, for 2.0 wt % pNIPAm−AAc microgel dispersions at pH 3.5 as a function of aging time. Note that the first $g(r)$ peak for the fluid phases (1 and 5 days after preparation) corresponds to the hydrodynamic diameter of microgel particles, whereas the first peak for the crystalline phase (11 and 27 days after preparation) corresponds to the lattice constant of colloidal crystals. The black vertical dashed line corresponds to the hydrodynamic diameter of the microgels determined in the dilute limit.

as opposed to the transient cages observed in the fluid phase. However, even in the crystalline phase, the microgel assemblies still age with time, which is manifest by the continual slowing of the dynamics with sample aging. The plot of β versus aging time t (Figure 4b) provides a semiquantitative representation of the aging of these dispersions.[38]

As illustrated by the images shown in Figures 2 and 3, the structure of microgel assemblies evolves as the dynamics of the particles slows. Figure 5 illustrates this relationship in terms of the radial distribution function [$g(r)$] for pNIPAm−AAc microgel assemblies (2.0 wt % polymer in pH 3.5 buffer) as a function of the number of days after sample preparation. In general, the first peak in the $g(r)$ plot for a fluid phase is equal to the diameter of the particles,[39,40] whereas for a crystalline phase, the first peak represents the mean particle center-to-center distance.[41] One day after sample preparation, the $g(r)$ plot has relatively weak structure, with only the first two peaks being easily identified. In very dilute (0.01 vol %) dispersions at pH 3.5, the pNIPAm−AAc microgel particles have a hydrodynamic diameter of 2.1 μm (from particle tracking microrheology; see below and in the Supporting Information). However, in the freshly prepared 2.0 wt % microgel sample, the interparticle distance is only about 1.9 μm, as determined from the first peak in the $g(r)$ plot. The particle size in the dispersion is presumably smaller than the hydrodynamic diameter measured under highly dilute conditions (2.1 μm) because of the previously observed osmotic deswelling of the microgels,[9,23] which occurs when the polymer concentration is increased beyond the dilute regime.[23,42] In this case, osmotic deswelling significantly decreases the effective volume fraction of the microgels from 56% to 41% (see eq 8), which is too dilute to produce long-range crystalline order for interparticle interactions that are dominated by mutual volume exclusion only.

These data also suggest that the particle size increases with aging even in the fluid phase, which is evident from the fact that the apparent particle size after 5 days of aging is slightly larger than that observed after 1 day. After 10 days, the microgel particles self-assembled into colloidal crystals, which are clearly observed in the $g(r)$ plots by a dramatic increase in structure at larger values of r. After the samples had been aged for 27 days, the interparticle distance increased to 2.3 μm, which is slightly greater than the hydrodynamic diameter determined under dilute conditions (2.1 μm). Whereas the changes occurring at the

molecular scale that result in the observed aging of our assemblies are still not clear, it seems likely that the decrease in particle dynamics over such long times is the result of a slow progression to a system with strongly attractive interparticle interactions. As we have suggested before, it might be the case that the microgel particles swell as a result of the formation of multiple interparticle hydrogen bonds between the protonated carboxylic acid groups and/or amide groups, which decreases the configurational entropy of the polymeric chains while increasing the enthalpic contribution to particle assembly.[5,6,9,27] With the pairwise interactions between the particles apparently being very weak, as evidenced by the lack of aggregation in the dispersions, it is likely that multibody interactions are required to form the crystalline assembly. The rearrangement of polymeric segments on multiple neighboring particles (particle swelling and interdigitation) to optimize both the number and orientation of the hydrogen bonds and concomitant multibody interactions between particles might favor particle swelling in order to minimize the local Gibbs free energy.[6]

Our speculation that attractive interparticle interaction potentials might drive the phase transition with aging can conceivably be probed in a more direct manner. For example, colloidal interaction potentials have been measured directly by optical tweezers,[43] total internal reflection microscopy,[44] and atomic force microscopy techniques,[45] Herein, we use the thermostability of the colloidal assemblies as an indirect in situ indicator of interparticle interactions between pNIPAm−AAc microgel particles in the context of their instantaneous phase behavior and their aging history. Reports by Senff and Richtering,[3] Wu et al.,[8] and St. John et al.[9] have illustrated that, for purely repulsive microgel crystals, melting will occur at a temperature slightly below the intrinsic LCST of the microgel particles comprising the assembly. As the temperature is raised, the microgels deswell enough to drive the volume fraction of the assembly from the crystalline region of the phase diagram to the fluid region. Therefore, the thermal stability of a microgel dispersion should report on the interparticle interactions, with the assembly becoming more thermally stable if multibody interparticle attractive interactions are present; the additional enthalpic contribution to the assembly will represent an additional energy barrier that must be overcome to drive assembly melting.

Figure 6 presents the thermal melting behavior of 2.0 wt % pNIPAm−AAc microgel dispersions in pH 3.5 buffer as a function of sample age. We quantitatively assess crystal melting using the phenomenological Lindemann criterion. The quasi-two-dimensional time-dependent Lindemann parameter is defined as

$$\gamma_L(\tau) = \frac{\sqrt{\mathrm{MSD}(\tau)}}{a} \qquad (4)$$

where a is the ensemble-averaged center-to-center distance between particles.[6,46,47] The quasi-two-dimensional Lindemann parameter is a measurement of time-dependent positional fluctuations of microgel particles relative to the crystal lattice spacing. From the data presented in Figure 6, the thermal stability of microgel dispersions clearly increases with age. After 1 day of sample aging, the time-dependent Lindemann parameter, $\gamma_L(\tau)$, is roughly linear with lag time, and at all temperatures from 20 to 39.9 °C, the maximum Lindemann parameters are greater than the critical melting Lindemann parameter [0.16 for a face-centered cubic (fcc) lattice]. For the 1-day-old sample, it is interesting to notice that there is a marked decrease in the

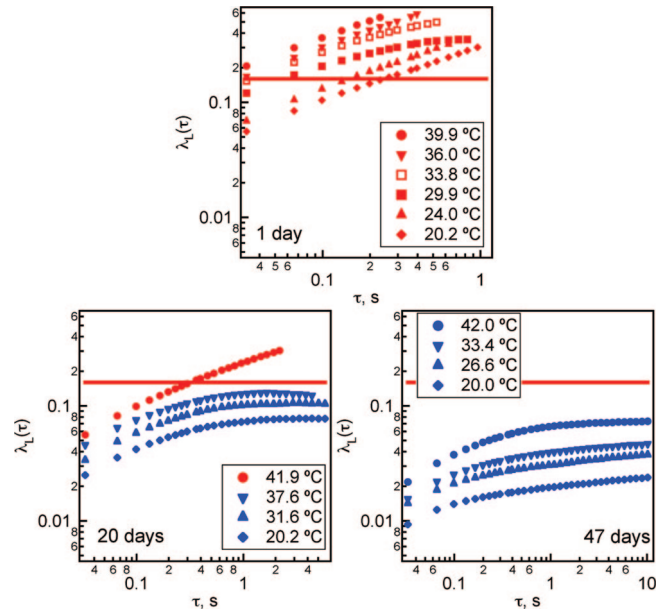

Figure 6. Age-dependent thermal stability of 2.0 wt % pNIPAm−AAc microgel dispersions in pH 3.5 buffer. Red symbols indicate fluid microgel dispersions, whereas blue symbols represent crystalline behavior. The age of each sample is indicated on each plot of the Lindemann parameter [$\gamma_L(\tau)$] versus lag time (τ). The horizontal red line in each frame is the critical Lindemann parameter for crystal melting ($\gamma_L^{max} = 0.16$).

particle dynamics when the temperature is raised to 30 °C. This arises from weak, transient particle aggregation, where the hydrophobic interaction between the deswollen microgels begins to dominate over electrosteric repulsion. Particle aggregation is also evident in the $g(r)$ plots (data not shown) and an increase in sample turbidity. However, as temperature continues to increase to 36 °C, the thermal energy of the particles dominates over interparticle attractions, thereby resulting in a recovery of diffusive behavior. After 20 days of aging, the microgel dispersion is largely crystalline with some regions of fluid coexistence. At this point, the crystalline phase displays melting at approximately 40 °C as shown in Figure 6. Note that this temperature is far above the LCST of pNIPAm−AAc microgels at this pH (~32 °C), reflecting the onset of attractive interparticle interactions. The 47-day-aged sample, which is completely crystallized, was not observed to melt even when the temperature was raised to 42 °C, which is the highest temperature our instrument allows. Indeed, the particles were still strongly caged and appeared to be in close contact with one another, with the maximum Lindemann parameter being nearly a factor of 10 lower than the melting value, reflecting an extremely stable assembly. These data clearly indicate that the aging process is associated with the evolution of attractive interactions between neighboring microgel particles, which effectively increases the LCST value for the particles when they are placed in the context of an aged colloidal assembly.

So far, we have focused on only the aging and phase behavior pNIPAm−AAc microgel dispersions at pH 3.5, as these assemblies age very slowly, thereby permitting convenient monitoring of the aging process by microscopy. However, it is known that pNIPAm−AAc microgel particles are both thermoresponsive, displaying a volume phase transition at ~32 °C (when the AAc groups are largely protonated), and pH-responsive, with the AAc moieties having a pK_a of ~4.3. Thus, it is expected that the phase behavior will be pH-dependent, at least with respect to the volume exclusion of the particles. To

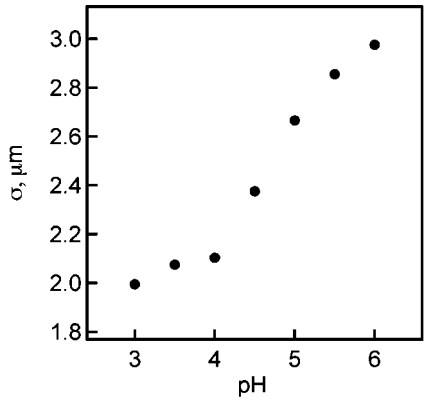

Figure 7. Hydrodynamic diameter of pNIPAm−AAc microgel particles measured by video microscopy at 0.01 wt % in buffers with pH values ranging from 3.0 to 6.0 at 20 °C.

determine the change in particle size as a function of pH, we used video-microscopy-based particle tracking. This technique allows for the direct, real-space measurement of diffusion coefficients and is straightforward for particles larger than the diffraction limit. Note that ensemble-averaged techniques such as dynamic light scattering were difficult to apply reliably for these larger particles because of large number density fluctuations observed in the dilute regime, which introduce significant error into the measurements.

The hydrodynamic diameters of microgel particles (σ) were obtained using the following scheme: Very dilute (0.01 wt %) microgel suspensions were tracked by video microscopy to obtain linear MSD vs τ plots; because dilute dispersions exhibit unhindered diffusion, the translational self-diffusion coefficient D can be extracted from the slope of this plot by using eq 5 if the vertical (out-of-plane) motion of particles is ignored[6,9]

$$D = \frac{\mathrm{d}[\mathrm{MSD}(\tau)]}{\mathrm{d}\tau}/2d \tag{5}$$

Combining this equation with the Stokes−Einstein equation

$$D = \frac{k_\mathrm{B}T}{d\pi\sigma\eta_\mathrm{s}} \tag{6}$$

yields an expression from which the hydrodynamic diameter (σ) in the dilute regime can be obtained

$$\sigma = \frac{2k_\mathrm{B}T}{\pi\eta_\mathrm{s}\dfrac{\mathrm{d}[\mathrm{MSD}(\tau)]}{\mathrm{d}\tau}} \tag{7}$$

where k_B is the Boltzmann constant, T is the absolute temperature, d[MSD(τ)]/dτ is the slope of the linear portion of the MSD vs τ plot, and η_s is the intrinsic viscosity of the solvent. The thus-determined hydrodynamic diameters of pNIPAm−AAc particles from pH 3.0 to pH 6.0 at 20 °C are displayed in Figure 7. From these data, we observe an increase in diameter from ~2.0 μm at pH 3.0 to ~3.0 μm at pH 6.0, with the approximate inflection point at pH ~4.5, in reasonable agreement with the typical pK_a for the acrylic acid monomer (~4.3). Note that this increase in charge density is also reflected in the pH-dependent electrophoretic mobility (see the Supporting Information).

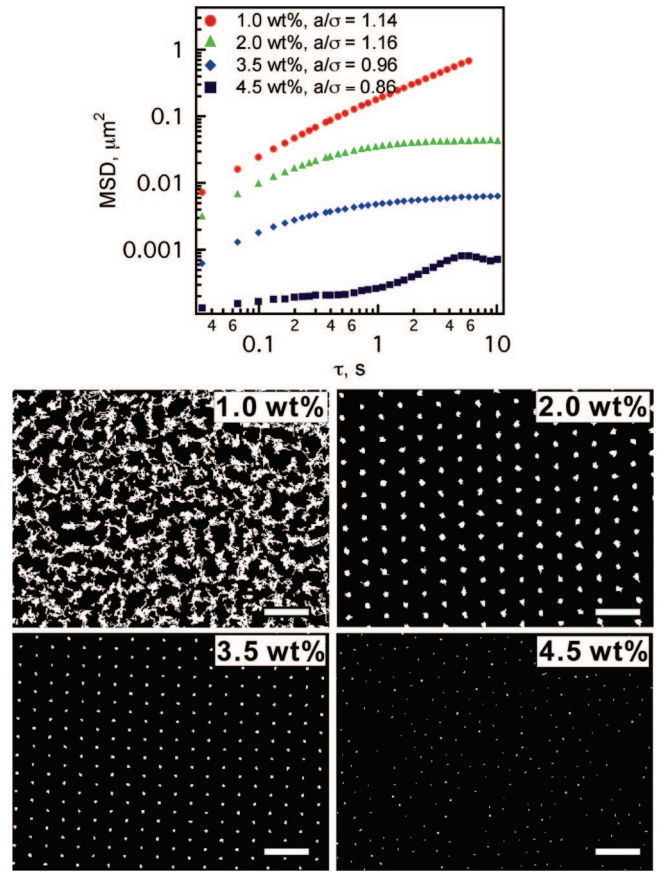

Figure 8. Concentration-dependent phase behavior of microgels at pH 3.0 and 20 °C, approximately 30 days after sample preparation. The double-logarithmic plot of MSD vs τ is shown in the top panel, and the weight concentrations are indicated in the legend. The bottom panels contain trajectories of microgel assemblies over ~10 s of observation for weight percentages ranging from 1.0 to 4.5 wt %. Scale bar = 5 μm.

As suggested above, the large magnitude of swelling that occurs as a function of pH should result in dispersion phase behavior that is similarly pH-dependent. At lower pH values, because each particle occupies a smaller volume, it is expected that pNIPAm−AAc particles will assemble into colloidal crystals or glasses at higher weight fractions than observed at higher pH values, where the particle volume is greater. This is clearly seen in Figures 8 and 9, which illustrate the progression of phase behavior at pH 3.0 (Figure 8) and pH 5.0 (Figure 9) as a function of polymer (microgel) weight fraction following ~30 days of aging. Figure 8 presents the double-logarithmic plot of MSD vs τ for pNIPAm−AAc microgels at pH 3.0 and 20 °C with increasing concentration. As the concentration of particles is increased, the dispersion progresses through a typical fluid → crystal → glass transition.[4] At 0.5 wt %, the microgel dispersion remains in the fluid phase even after aging, where $\beta \approx 1$, indicating diffusive motion. When the microgel concentration reaches 1.5 wt %, the microgels form a crystalline phase, and the MSD reaches a plateau after an initial increase, indicating that the microgels are caged in fixed lattice sites. When the particle concentration is raised above 4.0 wt %, the microgels are compressed together in a confined arrangement and tend to form a random glassy phase. Under these conditions, microgel diffusion is too frustrated for an ordered crystalline lattice to form. Note that polycrystalline and crystal/glass coexistence phases are observed in some high-concentration samples; for simplicity, we refer to samples that are largely frozen in a disordered configuration as "glassy".

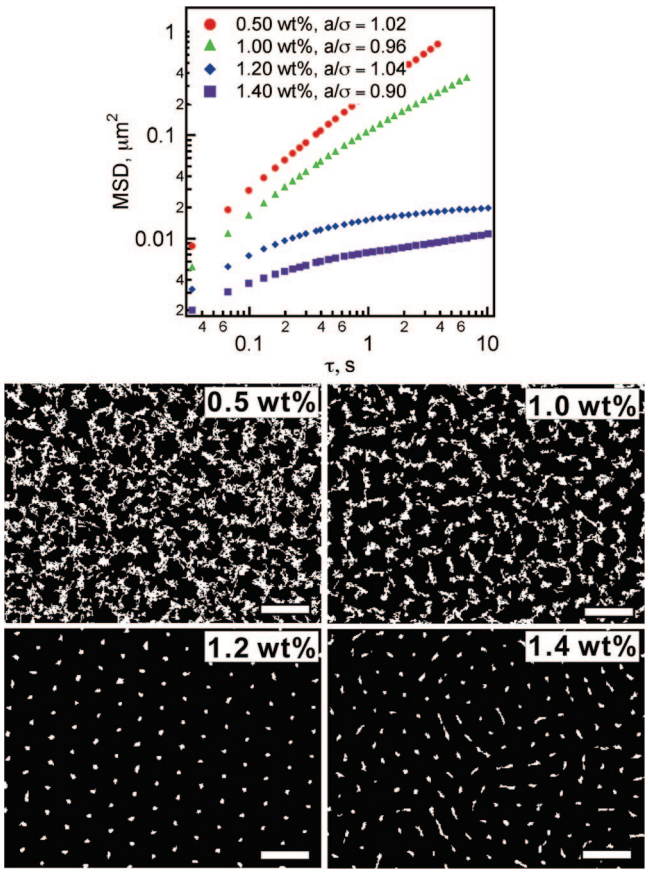

Figure 9. Concentration-dependent phase behavior of microgels at pH 5.0 and 20 °C, approximately 30 days after sample preparation. The top panel is a double-logarithmic plot of MSD vs τ. The bottom panels contain trajectories over ~10 s of observation for microgel assemblies at weight percentages ranging from 0.5 to 1.4 wt %. Scale bar = 5 μm.

Analogous phase transitions are observed for microgel dispersions at pH 5.0, albeit at very different concentrations. As shown in Figure 9, at 0.5 wt %, the sample is in a fluid phase, as was observed for the pH 3.0 sample. However, the trajectories at pH 5.0 show less mobility than those observed at the lower pH, as illustrated by the fact that the MSD values are significantly smaller than those observed at pH 3.0. Also, a subtle curvature is observed in the 0.5 wt % MSD plot at long lag times, suggesting that the microgel motion is slightly subdiffusive. At 1.0 wt %, the particle motion slows, the MSD plot shows more pronounced curvature, and the trajectories are clearly less diffusive than those for the 0.5 wt % sample. Increasing the concentration to 1.2 wt % results in the assembly of the microgels into a crystalline phase in which the MSD reaches a plateau after an initial increase. A further increase in microgel concentration to 1.4 wt % results in a partially disordered glassy/crystalline sample. The data presented in Figures 8 and 9 are representative of the expected phenomenon: swelling of microgel particles with increasing pH results in transitions to crystalline and glassy states at lower weight percentages.

To place these observations in an experimental framework commensurate with previous work on hard-sphere packing,[40] it is necessary to express the microgel concentration in terms of volume fraction, which is the typical control parameter used for hard spheres. Because of the extreme amount of solvent swelling observed in pNIPAm−AAc microgels, it is difficult to directly determine the volume fraction from the weight fraction, given that the density of the individual microgels varies with concentration and pH and is difficult to measure directly.[3] It is also difficult to measure the diameters of microgel particles precisely in situ through direct microscopic imaging because of the diffraction limit.[48] We and others[3,5,9] have previously addressed this issue by extrapolating packing fractions from shift factors obtained in the dilute regime through rheological measurements on dispersions. However, this approach is likely to be valid only in the case of purely repulsive hard spheres, which, given the results presented above, clearly is not an appropriate assumption for the system under study. Therefore, we used only the rheology method for samples that remained in the fluid regime after aging, in which the volume fraction can be estimated by multiplying the weight fraction by the appropriate shift factor for each pH.[3] In the crystalline and glassy phases, the volume fraction is represented as the ratio of the average microgel center-to-center distance (a) in concentrated dispersions to the microgel hydrodynamic diameter in dilute dispersions (σ, see Figure 7). The average center-to-center distance (a) was obtained from the first peak in the radial distribution function $g(r)$, which was obtained from analysis of the microscopy images. From these data, one can determine the effective volume fractions in the crystalline and glassy phases, as it is known that the volume fraction for closest packing is 0.740 ($2^{1/2}\pi/6$) in a face-centered cubic (fcc) or hexagonal close-packed (hcp) lattice. If we assume that the crystalline packing of microgel particles is fcc, the effective volume fraction of microgels (Φ_{eff}) will scale with a/σ by

$$\Phi_{eff} = \frac{0.740}{(a/\sigma)^3} \tag{8}$$

Therefore, for hard spheres, the freezing transition at $\Phi_f = 0.494$ corresponds to $(a/\sigma)_f = 1.14$, whereas the melting transition at $\Phi_m = 0.545$ corresponds to $(a/\sigma)_m = 1.11$. It is critical to note that, for hard spheres, a/σ can never be less than 1, as rigid particles cannot be compressed, whereas for soft spheres such as pNIPAm−AAc microgels, a/σ can have values much less than unity because of the intrinsic compressibility of microgels. Thus, by the above treatment, the "effective" volume fraction of microgels can be greater than 0.740 when $a/\sigma < 1$, equivalent to compression of all microgel particles. It is also noteworthy to mention that, for random closest packing, as would be found in a Bernal glass, the maximum volume fraction is 0.64.[49,50] Therefore, for systems that either are completely glassy or display glass/crystal coexistence, the volume fraction will lie between 0.64 and 0.74, and eq 8 will overestimate the effective volume fraction. Furthermore, we have never observed any evidence of particle deformation from a spherical shape; the actual close-packing limit is therefore not be expected to be much higher than 0.74.

Given this approach, the experimentally determined phase diagram for pNIPAm−AAc microgel suspensions following ~30 days of aging is displayed in Figure 10, in which the left vertical axis represents a/σ and the right vertical axis denotes the effective volume fraction Φ. At each pH value (with constant ionic strength), a series of microgel dispersions with increasing weight fractions were prepared, and the microgel dynamics were recorded as described above to construct the phase diagram. In line with the more detailed data in Figures 8 and 9, the phase diagram shows that a decrease in a/σ (increase in volume fraction) at a fixed pH is accompanied by a fluid → crystal → glass transition, similar to the phase behavior for repulsive hard spheres[40,51] and simple pNIPAm colloids.[3,4] However, the

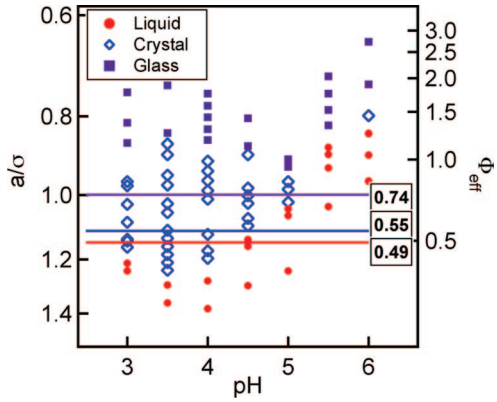

Figure 10. Phase diagram of pNIPAm−AAc microgels as a function of pH after ~30 days of aging. The volume fraction of microgels in suspension is scaled by the ratio between the center-to-center distance between microgels (a) and the dilute solution diameter of the microgels (σ) as a function of pH. Red circles represent the fluid phase, blue diamonds represent the crystalline phase, and magenta squares represent the glassy phase. The red, blue, and magenta horizontal lines represent the hard-sphere freezing, melting, and maximum-packing volume fractions, respectively.

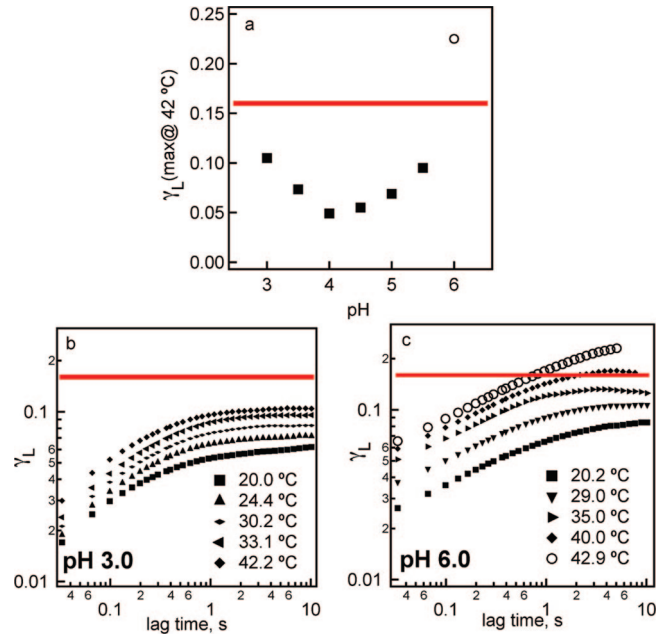

Figure 11. (a) Maximum time-dependent Lindemann parameter ($\gamma_L^{max@42°C}$) of pNIPAm−AAc microgels at 42.0 °C from pH 3.0 to 6.0. The weight percentage for each pH is 2.0 wt % for pH 3.0, 3.5, 4.0, and 4.5; 1.2 wt % for pH 5.0; and 1.1% for pH 5.5 and 6.0. (b,c) Time-dependent Lindemann parameter [$\gamma_L(\tau)$] of pNIPAm−AAc microgels at different temperatures at pH (b) 3.0 and (c) 6.0. The horizontal red lines represent the critical Lindemann parameter, 0.16, which is the melting point of fcc or hcp-type crystals. Solid symbols represent solid-phase samples, whereas open symbols represent fluid phases.

similarity to hard spheres is not quantitative when considering the canonical phase transitions for that system. The typical phase boundaries are superimposed on the experimental data in Figure 10 ($\Phi_f = 0.494$, $\Phi_m = 0.545$, and $\Phi_{max} = 0.74$); by and large, the observed transitions for the microgel dispersions are very different from those found for hard spheres. For example, at very low effective volume fractions ($\Phi_{eff} = 0.40$, corresponding to $a/\sigma = 1.22$) crystallization was observed at pH 3.0, 3.5, and 4.0 after aging. Conversely, dispersions remained fluidlike at pH 5.5 and 6.0 even above the close-packing limit ($a/\sigma = 1$). These values are also very dissimilar from those measured for simple pNIPAm colloids, for which crystallization has been observed for $\Phi_{eff} = 0.56-0.63$.[3,4] The general trend displayed in Figure 10 is that the pNIPAm−AAc microgels apparently crystallize at much lower Φ_{eff} values under acidic conditions (pH < pK_a) and are too compressible to form crystals at higher pH values (pH > pK_a), along with fluidlike mobility at high packing fractions. As we suggested above and in previous publications,[5,6] one possible explanation for this odd phase behavior centers around the AAc moieties in the pNIPAm−AAc microgels. For example, in the case of pH 3.0, only 5% of AAc moieties are ionized, and the Coulombic repulsion and internal osmotic pressure of microgel particles are thus much smaller than at higher pH values. Because of the moderate ionic strength, which was kept constant at 10 mM in all samples, the Debye−Hückel screening length is rather short, with an estimated value of ~3 nm. Under these conditions, acid−acid and acid−amide hydrogen bonding between particles should be maximized, thereby potentially resulting in a net attractive interaction at short particle separations. Conversely, as the pH is increased, the degree of AAc ionization increases (see Figure 7 and the Supporting Information), causing not only microgel swelling but also an increased Coulombic repulsion between particles, at least over short distances. Apparently, under these conditions, crystallization is frustrated, and the dispersions remain fluid up to very high volume fractions. Similar effects were observed for highly charged, ultrasoft microgels by Weitz and co-workers.[52] In those experiments, mechanical particle deformation was invoked as the main mechanism by which the particles diffused by each other in concentrated dispersions. Whereas we cannot precisely determine whether this is occurring by microscopy because of the limited optical resolution of our apparatus, we do not see strong evidence for this behavior from microscopy. It might be the case, however, that transient deformation is occurring that permits particle motion to be diffusive even at high concentrations.

As with the aging experiments described above, thermostability measurements of pNIPAm−AAc microgel colloidal crystals provide additional information regarding the nature of the interactions as a function of pH. Figure 11a shows the maximum Lindemann parameter ($\gamma_L^{max@42°C}$) measured at a temperature of 42 °C for pNIPAm−AAc dispersions as a function of pH. Note that this temperature represents the upper limit for our objective heater; direct microscopic observation of melting in all samples with accurate temperature control is not possible with our current equipment because of this limitation. In this figure, we show the results obtained for dispersions with weight fractions near the lower limit for crystallization at each pH value. Thus, these data represent the "weakest" assemblies formed at each pH. The thick red line represents the critical Lindemann parameter for fcc latticce melting, $\gamma_L^c = 0.16$. We observe that the $\gamma_L^{max@42°C}$ values for pNIPAm−AAc crystals from pH 3.0 to 5.5 are well below the critical Lindemann parameter for melting. The only sample that melts below 42 °C is the one formed at pH 6.0, for which melting of the pNIPAm−AAc assembly and formation of the fluid phase is quantitatively confirmed by the Lindemann parameter of 0.23 at 42 °C. The time-dependent Lindemann parameters of dispersions at different temperatures in pH 3.0 and pH 6.0 buffers are shown in Figure 11b,c, respectively. For colloidal crystals at pH 3.0, the particle motion remains caged even at temperatures much higher than the intrinsic volume phase transition temperature (VPTT) of pNIPAm−AAc microgels at this pH (~32 °C). As was discussed above, the marked thermostability of the pNIPAm−AAc colloidal crystals suggests

that significant enthalpic, attractive interparticle interactions exist in these microgel assemblies. These attractions presumably can be attributed to hydrogen bonding[6] and/or hydrophobic interactions at temperature above the VPTT.[53] In Figure 11c, the time-dependent Lindemann values are also shown for a caged pNIPAm−AAc dispersion (1.4 wt %) at pH 6.0. In this case, the assembly actually melts at a temperature of ∼40 °C, which is *lower* than the intrinsic VPTT of pNIPAm−AAc microgels at this pH (∼50 °C).[54] This sub-LCST melting behavior is typical for microgel crystals with purely repulsive interactions, as described previously.[5,8,9] Thus, in contrast to the other data shown in Figure 11, the thermally induced melting of the pNIPAm−AAc crystalline phase at pH 6.0 suggests that repulsive interactions dominate at this pH, where hydrogen bonding is frustrated by AAc deprotonation. The pH 6.0 results mirror those previously obtained on purely repulsive, thermosensitive microgel dispersions, where small amounts of microgel deswelling resulted in melting of the crystalline phase.[9] In contrast, the thermostable phases observed at lower pH values cannot be explained by repulsive potentials; an additional stabilizing force must be present in such assemblies. Together, these data suggest that the pH tunability of these microgel dispersions arises not only from particle volume changes, but also from modulation of the interparticle interactions, which evolve slowly, presumably as the result of a subtle competition between inter- and intraparticle chain−chain interactions.

Conclusions

We have directly observed aging during the self-assembly of pNIPAm−AAc microgel particles in a closed system. During this aging process, the microgel dynamics slows; the microgel diameters increase; and the mean interaction potential between particles becomes more attractive, which stabilizes the thus-formed colloidal crystals against thermal melting. Our results also suggest that the crystallization process is convolved with aging, where the slowing dynamics of the dispersion is synergistic with crystallization because of an increase in particle volume fraction with time. Additionally, although the molecular origins of aging are not yet clear, our data suggest that microgel dispersions evolve through a slow reconfiguration of the system from one that is dominated by intraparticle (polymer−polymer) interactions to one that is dominated by multibody interparticle interactions. This effect is perhaps most clearly seen in Figure 5, where the microgels appear to be in a somewhat condensed state immediately after sample preparation, which leads to fluid behavior. Over time, however, the particles appear to swell, as evidenced by the shift in the $g(r)$ plot to larger values of r. Thermostability experiments confirmed that this aging process is accompanied by the evolution of attractive interparticle forces.

The phase behavior that evolves during aging also suggests that attractive interactions are at work. When the pH of the suspension medium is lower than the AAc pK_a, the pNIPAm−AAc microgel particles form colloidal crystals at volume fractions as low as 40% (pH 3.0), which is probably due to hydrogen bonding and/or multibody interactions between particles, as we have described previously.[6] Because of the delicate balance between repulsive and attractive interactions between particles, the formation of colloidal crystals becomes more favored when the pH is close to the AAc pK_a, at which point the volume fraction for crystallization spans from 40% to over 100% (indicating the compression of particles under dense packing conditions). Finally, when the pH is above the AAc pK_a, the deprotonated AAc segments do not form hydrogen bonds efficiently, thereby shutting down a source of attractive interactions. It also appears that, under these conditions, the pNIPAm−AAc particles are so deformable that crystallization is frustrated and the dispersion prefers to remain fluid even at very high packing fractions (>100%). Together, these results illustrate the incredibly rich physics and dynamic nature found in this colloidal system. Despite the extensive amount of experimentation carried out in these studies, it is likely that we have only scratched the surface and that deeper studies of these phenomena will produce additional observations that speak to the complex interplay between colloidal and polymer energetics.

Acknowledgment. L.A.L. acknowledges financial support from the Dreyfus Foundation, the Office of Naval Research (ONR), and the ONR DURIP program for this work (N00014-03-1-0225 and N00014-04-1-0488). V.B. acknowledges support from the National Science Foundation (CAREER award, CTS-0547066).

Supporting Information Available: Experimental section and plot of the microgel zeta potential as a function of pH. This material is available free of charge via the Internet at http://pubs.acs.org/.

References and Notes

(1) Weeks, E. R.; Weitz, D. A. *Phys. Rev. Lett.* **2002**, *89* (9), 4.
(2) Yodh, A. G.; Lin, K.-H.; Crocker, J. C.; Dinsmore, A. D.; Verma, R.; Kaplan, P. D. *Philos. Trans. R. Soc. A* **2001**, *359* (1782), 921–937.
(3) Senff, H.; Richtering, W. *J. Chem. Phys.* **1999**, *111* (4), 1705–1711.
(4) Gao, J.; Hu, Z. *Langmuir* **2002**, *18*, 1360–1367.
(5) Debord, S. B.; Lyon, L. A. *J. Phys. Chem. B* **2003**, *107* (13), 2927–2932.
(6) Meng, Z.; Cho, J. K.; Debord, S.; Breedveld, V.; Lyon, L. A. *J. Phys. Chem. B* **2007**, *111*, 6992–6997.
(7) Watzlawek, M.; Likos, C. N.; Löwen, H. *Phys. Rev. Lett.* **1999**, *82*, 5289–5292.
(8) Wu, J.; Zhou, B.; Hu, Z. *Phys. Rev. Lett.* **2003**, *90*, 048304.
(9) St. John, A. N.; Breedveld, V.; Lyon, L. A. *J. Phys. Chem. B* **2007**, *111* (27), 7796–7801.
(10) Kratz, K.; Hellweg, T.; Eimer, W. *Ber. Bunsen-Ges. Phys. Chem.* **1998**, *102*, 1603–1608.
(11) Kokufuta, E.; Wang, B.; Yoshida, R.; Khokhlov, A. R.; Hirata, M. *Macromolecules* **1998**, *31*, 6878–6884.
(12) Weiss, J. A.; Larsen, A. E.; Grier, D. G. *J. Chem. Phys.* **1998**, *109* (19), 8659–8666.
(13) Dai, S.; Ravi, P.; Tam, K. C. *Soft Matter* **2008**, *4*, 435–449.
(14) Tan, B. H.; Tam, K. C. *Adv. Colloid Interface Sci.* **2008**, *136*, 25–44.
(15) Valignat, M.-P.; Theodoly, O.; Crocker, J. C.; Russel, W. B.; Chaikin, P. M. *Proc. Natl. Acad. Sci. U.S.A.* **2005**, *102* (12), 4225–4229.
(16) Pelton, R. *Adv. Colloid Interface Sci.* **2000**, *85*, 1–33.
(17) Sieglaff, C. L. *Polymer* **1963**, *4* (2), 281–284.
(18) Shashoua, V. E.; Beaman, R. G. *J. Polym. Sci.* **1958**, *33* (126), 101–117.
(19) Staudinger, H.; Husemann, E. *Ber. Chem.* **1935**, *68* (8), 1618–1634.
(20) Baker, W. O. *Ind. Eng. Chem. (Washington D. C.)* **1949**, *41*, 511–520.
(21) Dinsmore, A. D.; Prasad, V.; Wong, I. Y.; Weitz, D. A. *Phys. Rev. Lett.* **2006**, *96*, 185502−1185502−4.
(22) Bartsch, E.; Kirsch, S.; Lindner, P.; Scherer, T.; Stölken, S. *Ber. Bunsen-Ges. Phys. Chem.* **1998**, *102*, 1597–1602.
(23) Tan, B. H.; Tam, K. C.; Lam, Y. C.; Tan, C. B. *Langmuir* **2005**, *21* (10), 4283–4290.
(24) Das, M.; Kumacheva, E. *Colloid Polym. Sci.* **2006**, *284*, 1073–1084.
(25) Heskins, M.; Guillet, J. E. *J. Macromol. Sci. Chem.* **1968**, *A2*, 1441–1455.
(26) Pelton, R. H.; Chibante, P. *Colloids Surf.* **1986**, *20*, 247–256.
(27) Debord, J. D.; Lyon, L. A. *J. Phys. Chem. B* **2000**, *104* (27), 6327–6331.
(28) Lyon, L. A.; Debord, J. D.; Debord, S. B.; Jones, C. D.; McGrath, J. G.; Serpe, M. J. *J. Phys. Chem. B* **2004**, *108*, 19099–19108.
(29) Tsuji, S.; Kawaguchi, H. *Langmuir* **2005**, *21* (18), 8439–8442.
(30) Holtz, J. H.; Holtz, J. S. W.; Munro, C. H.; Asher, S. A. *Anal. Chem.* **1998**, *70* (4), 780–791.
(31) Holtz, J. H.; Asher, S. A. *Nature* **1997**, *389* (6653), 829–832.

(32) Das, M.; Zhang, H.; Kumacheva, E. *Annu. Rev. Mater. Res.* **2006**, *36*, 117–142.

(33) Xu, S.; Zhang, J.; Paquet, C.; Lin, Y.; Kumacheva, E. *Adv. Funct. Mater.* **2003**, *13*, 468–472.

(34) Pham, K. N.; Puertas, A. M.; Bergenholtz, J.; Egelhaaf, S. U.; Moussaïd, A.; Pusey, P. N.; Schofield, A. B.; Cates, M. E.; Fuchs, M.; Poon, W. C. K. *Science* **2002**, *296*, 104–106.

(35) Snowden, M. J.; Chowdhry, B. Z.; Vincent, B.; Morris, G. E. *J. Chem. Soc., Faraday Trans.* **1996**, *92*, 5013–5016.

(36) Fernandez-Nieves, A.; Fernandez-Barbero, A.; Vincent, B.; de las Nieves, F. J. *J. Chem. Phys.* **2003**, *119* (19), 10383–10388.

(37) Saunders, B. R.; Vincent, B. *Prog. Colloid Polym. Sci.* **1997**, *105* (Trends in Colloid and Interface Science XI), 11–15.

(38) Wang, P.; Song, C. M.; Makse, H. A. *Nat. Phys.* **2006**, *2* (8), 526–531.

(39) Hansen, J. P.; McDonald, I. R. *Theory of Simple Liquids*, 4th ed.; Elsevier: Amsterdam, 2006.

(40) Pusey, P. N. Colloidal suspensions. In *Liquids, Freezing and Glass Transition*; Hansen, J. P., Levesque, D., Zinn-Justin, J., Eds.; North-Holland: Amsterdam, 1989; Vol. 51, pp 763−942.

(41) Israelachvili, J. N. *Intermolecular and Surface Forces*, 2nd ed.; Academic Press: London, U.K., 1991.

(42) Stieger, M.; Richtering, W.; Pedersen, J. S.; Lindner, P. *J. Chem. Phys.* **2004**, *120* (13), 6197–6206.

(43) Grier, D. G. *Curr. Opin. Colloid Interface Sci.* **1997**, *2*, 264–270.

(44) Prieve, D. C. *Adv. Colloid Interface Sci.* **1999**, *82* (1−3), 93–125.

(45) Toikka, G.; Hayes, R. A. *J. Colloid Interface Sci.* **1997**, *191* (1), 102–109.

(46) Alsayed, A. M.; Islam, M. F.; Zhang, J.; Collings, P. J.; Yodh, A. G. *Science* **2005**, *309*, 1207–1210.

(47) Saija, F.; Prestipino, S.; Giaquinta, P. V. *J. Chem. Phys.* **2006**, *124*, 244504.

(48) Baumgartl, J.; Bechinger, C. *Europhys. Lett.* **2005**, *71* (3), 487–493.

(49) Bernal, J. D. *Proc. R. Soc. London A* **1964**, *280* (1382), 299–322.

(50) Scott, G. D.; Kilgour, D. M. *J. Phys. D: Appl. Phys.* **1969**, *2* (6), 863.

(51) Pusey, P. N.; van Megen, W. *Nature* **1986**, *320*, 340–342.

(52) Cho, E. C.; Kim, J. W.; Fernandez-Nieves, A.; Weitz, D. A. *Nano Lett.* **2008**, *8* (1), 168–172.

(53) Ishida, N.; Kobayashi, M. *J. Colloid Interface Sci.* **2006**, *297*, 513–519.

(54) Kratz, K.; Hellweg, T.; Eimer, W. *Colloids Surf. A* **2000**, *170*, 137–149.

JP8104979